El Niño and droughts in Southeast Asia: A stochastic-chaotic modeling approach

Davide Faranda, Yuzuru Sato, Chenyu Dong, Adriano Gualandi, Robin Noyelle, Tommaso Alberti, Berengere Dubrulle, Lucas Fery, Gabriele Messori, Mathieu Vrac, et al.

El Niño and Droughts in Southeast Asia: A Stochastic-Chaotic Modeling Approach

Davide Faranda,[1,2,3] Yuzuru Sato,[4,2] Chenyu Dong,[5] Adriano Gualandi,[6] Robin Noyelle,[1] Tommaso Alberti,[7] Berengere Dubrulle,[8] Lucas Fery,[8] Gabriele Messori,[9,10,11] Mathieu Vrac,[1] Pradeebane Vaittinada Ayar,[1] Pascal Yiou,[1] and Gianmarco Mengaldo[5]

[1] *Laboratoire des Sciences du Climat et de l'Environnement, UMR 8212 CEA-CNRS-UVSQ, Université Paris-Saclay & IPSL, CEA Saclay l'Orme des Merisiers, 91191, Gif-sur-Yvette, France*

[2] *London Mathematical Laboratory, 8 Margravine Gardens, London, W6 8RH, UK*

[3] *Laboratoire de Météorologie Dynamique/IPSL, École Normale Supérieure, PSL Research University, Sorbonne Université, École Polytechnique, IP Paris, CNRS, 75005, Paris, France**

[4] *Complex Systems Research Group, RIES / Department of Mathematics, Hokkaido University, Kita 12 Nishi 7, Kita-ku, Sapporo, Hokkaido 060-0812, Japan*

[5] *National University Singapore, Singapore*

[6] *University of Cambridge, UK*

[7] *Istituto Nazionale di Geofisica e Vulcanologia, via di Vigna Murata 605, 00143, Rome, Italy*

[8] *SPEC, CEA, CNRS, Université Paris-Saclay, 91191, Gif-sur-Yvette, France*

[9] *Department of Earth Sciences, Uppsala University, Sweden*

[10] *Swedish Centre for Impacts of Climate Extremes (climes), Uppsala University, Sweden*

[11] *Department of Meteorology and Bolin Centre for Climate Research, Stockholm University, Sweden*

(Dated: February 5, 2025)

The El Niño-Southern Oscillation (ENSO) significantly impacts global weather, with strong El Niño events often linked to prolonged dry conditions in Southeast Asia. While some high-impact El Niño events have coincided with prolonged dry conditions, leading to droughts, the underlying causal mechanisms remain complex and inconsistent. In this study, we develop a minimal, data-driven model to quantify the conditions under which ENSO events amplify prolonged dry conditions risk in Southeast Asia. Unlike correlation-based approaches, our model identifies thresholds in sea surface temperatures and atmospheric patterns that increase the probability of prolonged dry conditions, highlighting both seasonal timing and intensity as critical factors. Our results show that when ENSO-induced anomalies exceed specific temperature and atmospheric thresholds, prolonged dry conditions probability rises significantly, aligning with observed historical droughts. Additionally, the model reveals periods where this link weakens due to competing regional climate factors, suggesting that certain conditions mitigate the typical ENSO-prolonged dry conditions connection. These findings provide a more nuanced understanding of ENSO-driven prolonged dry conditions variability, offering a probabilistic predictive framework with potential applications in climate adaptation, agricultural planning, and regional resource management.

I. INTRODUCTION

El Niño-Southern Oscillation (ENSO) is a naturally occurring climate phenomenon that affects weather patterns and precipitation across the globe [1]. ENSO is characterized by the cyclic warming and cooling of the tropical Pacific Ocean, which can lead to a wide range of impacts on global climate. El Niño (i.e. the positive phase of ENSO) which occurs when the sea surface temperature in the central and eastern Pacific is warmer than normal, is one of the most documented phases of ENSO [2].

* DF, YS, and CD contributed equally to this work. Correspondence to Davide Faranda (davide.faranda@cea.fr) & Gianmarco Mengaldo (mpegim@nus.edu.sg)

Southeast Asia (Fig. 1) is particularly vulnerable to the impact of El Niño events [3–6]. Some El Niño events (e.g., 1982-83 and 1997-98) have been known to cause prolonged dry conditions over this region leading to severe consequences for agriculture, water resources, and public health [7, 8]. In addition, global warming seems to exacerbate the anomalously warm surface air temperatures recorded during El Niño events, and it is debated whether it may change the frequency of El Niño events themselves [9, 10]. As a consequence, the frequency of prolonged dry conditions in Southeast Asia may also increase [11], potentially putting under more stress the region's ecological and societal systems. The IPCC states (see [12] WG1 Page 1597) that there is medium confidence that an increasing frequency of extreme (also referred to as strong) El Niño events will lead to an increasing frequency of prolonged dry periods in Southeast Asia.

El Niño events are considered strong (i.e., extreme) if the Niño3.4 index, depicted in Fig. 1a, exceeds the value of 1.5°. However, not all strong El Niño events are associated with prolonged dry conditions in Southeast Asia. In particular, the *non-systematic* relationship between strong El Niño and prolonged dry conditions represents a key open challenge in the literature, for which no mathematical model nor exhaustive explanation exists.

In this study, we propose a new model that uncovers a possible dynamical link between dry conditions in Southeast Asia and ENSO dynamics. To construct the new model, we first analyzed historical data of El Niño events and total column water vapor (that is highly correlated to total precipitation [13] while being more reliably represented in climate reanalysis data) patterns over Southeast Asia, using tools from dynamical systems theory and extreme value theory. Such techniques have been successfully used to characterize the dynamics of various complex systems, like a turbulent flow [14, 15], slow and laboratory earthquakes [16, 17], or the jet stream [18, 19], and they have been further developed to account for the spatial dimension [20], and better understand predictability [21].

This analysis allowed us to better understand the El Niño–precipitation system's long-term behavior and revealed some key dynamical properties, including the complexity and persistence of certain atmospheric configurations.

Based on these results, we introduced a new mathematical model that links dry and wet conditions in Southeast Asia with ENSO dynamics. The mathematical model couples the Jin-Timmermann equations describing ENSO dynamics [22, 23], defined in (1), with a stochastic Langevin model mimicking the wet-dry bi-stable dynamics, defined in (2b). The resulting stochastic system is described by four variables x, y, z and u. The first three belong to the Jin-Timmermann model and are non-dimensional versions of the ENSO strength, the Western Pacific temperature, and the oceanic circulation strength, respectively. The last variable, u, captures the wet-dry dynamics, and it is forced by the chaotic ENSO dynamics through the temperature anomaly over the Western Pacific (i.e., variable y in (1)) via (2b). For more details on the model, the interested reader may refer to Methods. Qualitatively, our model is in agreement with observations, and reveals a causal link between strong El Niño events and prolonged dry conditions over Southeast Asia, that matches its observed *non-systematic* nature. The new model enhances our understanding of the complex interaction between El Niño and prolonged dry conditions in Southeast Asia by identifying specific thresholds that elevate the risk of prolonged dry conditions. These insights contribute to refining probabilistic models, offering a stronger basis for assessing prolonged dry conditions likelihood in response to El Niño events, and better prepare for possible droughts.

II. ANALYSIS OF CLIMATE DATA

To investigate the dynamics of prolonged dry conditions in relation to ENSO, we use three datasets.

The first is the daily mean total column water vapour (TCWV) and the daily total precipitation (TP) over the tropical Indo-Pacific region [90°E–120°W,10°S–20°N] from the ERA5 reanalysis data over the period 1940-2022 [24]. TCWV is a key component of the water cycle in tropical regions [25], and contains information on both atmospheric dynamics and thermodynamics, including convection. In addition, it is closely connected to TP in the region as discussed in Supplementary Section 2. Despite TP being more directly linked to dry conditions, it presents some limitations if used as an observable when performing analysis based on dynamical systems approaches. Firstly,

reanalysis datasets have limitations in accurately capturing precipitation due to data assimilation constraints. These constraints arise from the inherent challenges in integrating diverse observational data sources, which can lead to biases and inaccuracies in precipitation estimates [26]. Secondly, TP is a non-smooth field, thus providing an extremely noisy dynamics in terms of phase-space reconstruction and dynamical systems analysis. Hence, TCWV is preferred for all the subsequent analyses relevant to dynamical systems presented in the rest of this paper.

The second dataset used is the monthly NOAA/ERSSTv5 Niño3.4 index, defined by Huang et al. [27], retrieved from the Royal Netherlands Meteorological Institute (KNMI) Climate Explorer.

Finally, the third dataset is the 3-month Standardized Precipitation Index (SPI-3) data derived from ERA5. This is used to describe dry conditions in Southeast Asia [28]. The yellow line in Fig. 2a represents the spatial average of SPI-3 over the land area within the Southeast Asia region (brown bounding box in Fig. 2c).

By comparing the SPI-3 and Niño3.4 indices in Fig. 1a), we observe that, consistent with previous studies, El Niño events are generally associated with drier-than-usual conditions in Southeast Asia [29]. However, this relationship is not systematic, as only a few strong El Niño events correspond with severe or prolonged dry conditions in the region. This drives us to further analyze the distinct dynamical characteristics of El Niño events through the lens of dynamical system theory.

For this purpose, we use two key dynamical indices: *local dimension* (d) and *persistence* (θ^{-1}), introduced in [30], detailed in [31] and described in detail in the Supplementary Information Section 1. Local dimension d quantifies the complexity of patterns in the variable of interest (TCWV in our case). In particular, it measures the number of active pattern components acting on a given field on a specific day, i.e., larger d suggests more active processes. Persistence θ^{-1} (in days), instead, measures how long a particular spatial pattern persists before transitioning to a different one. Results are shown in Fig. 1. In particular, Fig. 1a) displays the time series of the local dimension d (middle panel), and persistence θ^{-1} (bottom panel) for daily TCWV maps. While d and θ^{-1} time series mostly oscillate within a relatively narrow range, three time intervals (highlighted in darker grey) in 1982-83, 1997-98, and 2015-2016 show particularly low dimensions and high persistence. These correspond to three of the strongest El Niño events ever recorded in the past century. For d and θ^{-1}, we also display the 365-day moving average as a solid black line, where the peaks associated with strong El Niño events are more clearly visible.

When looking at the dimension-persistence diagram (Fig. 1b) as a function of the values of Niño3.4 index (colorscale), we observe a cluster of strong El Niño events showing high persistence of TCWV and low dimensions. To further explore the differences in dynamical properties between various El Niño events, we divide all days within the El Niño phase (represented by the shaded area in Fig. 1a) according to observed persistence. Specifically, we plot the composite anomalies for TCWV of the most persistent El Niño days (those in the upper quartile of persistence values) and the least persistent El Niño days (those in the lower quartile of persistence values) in Fig. 1c,d, respectively. The most persistent El Niño days display drier conditions than the least persistent El Niño days over Southeast Asia, as depicted in the composite anomalies maps (obtained by subtracting the daily seasonal cycle of each variable at each grid point). We present the composite anomaly maps of TP for the same two sets of days in Supplementary Fig. S2, with a very similar spatial configuration observed. The high correlation between TCWV and TP is further illustrated in Supplementary Fig. S1. In Supplementary Fig. S3, we additionally show the same results as Fig. 2, but using TP as observable. Despite some differences in the values of the dynamical indices and composite anomalies, the overall results are consistent with those obtained using TCWV. Fig. 1 highlights a nonlinear relationship between strong El Niño events and prolonged dry conditions. Notably, persistent TCWV configurations lead to more intense dry conditions over Southeast Asia, while less persistent patterns produce weaker anomalies. This analysis indicates that the data support the presence of an underlying, relatively low-dimensional attractor, structured into two basins of attraction. The dominant basin corresponds to wet conditions, while the less frequently visited basin represents prolonged dry conditions, characterized by a lower-dimensional, more persistent structure. We use this insight to develop the simplest model that replicates this behavior.

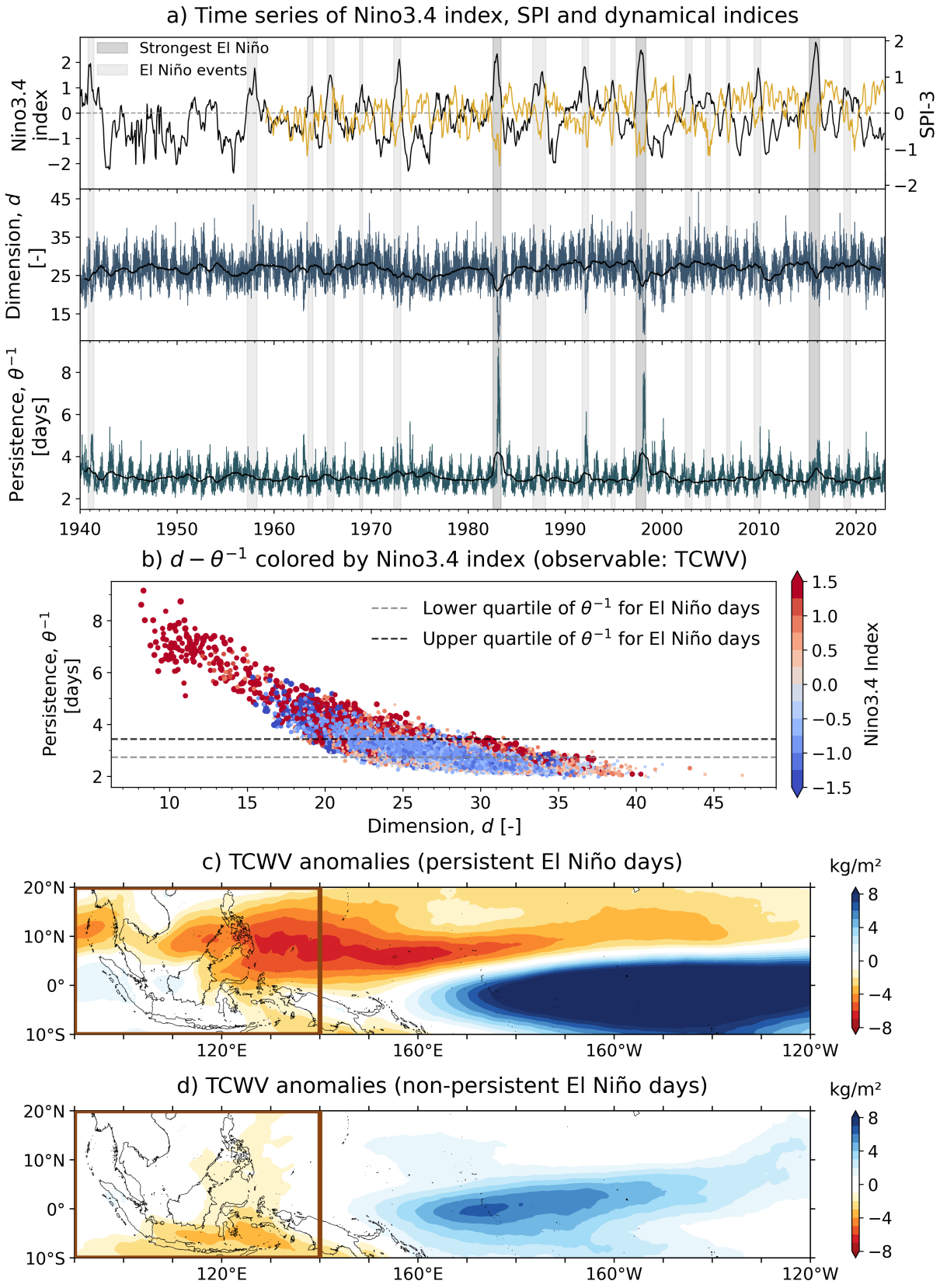

FIG. 1. **Dynamical analysis of the total column water vapour (TCWV) field from ERA5 data.** a) Time series of the spatially averaged 3-month Standardized Precipitation Index (SPI-3) (yellow) over Southeast Asia land (1959–2022) and the Niño3.4 index (black) (row 1), local dimension d (row 2), and persistence θ^{-1} (row 3). The 365-day moving averages for both dynamical indices are displayed as solid black lines. El Niño events are shown with light grey shading, while the strongest ones (1982-83, 1997-98, and 2015-2016) are highlighted in dark grey. b) Scatter plot of local dimension versus persistence, with each dot colored by the monthly values of the Niño3.4 index and sized by its absolute value. c) and d) show composite TCWV anomaly maps for persistent and non-persistent El Niño days, using the two thresholds from panel b). The brown bounding box [90°E–140°E, 10°S–20°N] represents the region used for computing the standardized anomaly shown in Fig. 2.

III. MODEL

To model the data, we follow the approach in [32] and construct the low-dimensional projection of the attractor. This low-dimensional projection is useful for capturing the essential dynamics of the climate system by reducing the complexity of the dataset while preserving key patterns of variability. First, we calculate the spatial average of TCWV anomalies over Southeast Asia within the bounding box shown in Fig. 1 [90°E–140°E, 10°S–20°N] and compute the average sea-surface temperature anomaly over the western equatorial Pacific [135°E–155°W, 5°S–5°N], as per Timmermann et al. [33]. We then detrend both time series and normalize by their standard deviations, yielding standardized daily anomalies of $TCWV(t)$ and $SST(t)$. A cubic polynomial is used for detrending to capture nonlinear trends, accommodating gradual changes or inflection points in the data. This allows us to isolate the underlying variability, focusing on the relationship between El Niño events and dry conditions.

We construct a 3-dimensional space with $TCWV(t)$, the Niño3.4 index $ENSO(t)$, and $SST(t)$, applying a moving average filter with a one year window to remove seasonal and sub-seasonal signals, following [34, 35]. The results are shown in Fig. 2a and the reconstructed attractor using the time series of $TP(t)$ is presented in Supplementary Fig. S4. A visual inspection of the reconstructed phase space reveals the presence of an attractor, indicating that water vapor dynamics in the tropical Indo-Pacific follows two states, representing two basins of attraction: i) a wet state, associated with a chaotic attractor (green states in Fig. 2a), and ii) a comparatively rare dry state (brown states in Fig. 2a). The fraction of very dry states (TCW$< -2\sigma$TCW, where σ is the standard deviation of TCW) over total number of states is 0.03.

We leverage this insight to create a first-order reduced model of precipitation over Southeast Asia, capturing the dynamics of dry and wet states through a stochastic model in a double-well potential modulated by ENSO dynamics. In the absence of El Niño, the potential is asymmetric, with the dry state less likely than the wet state, reflecting observations from Fig. 2a. During El Niño, the probability of the dry state increases, influenced by the duration of the El Niño phase. The system dynamics are described by the Jin-Timmermann model [23, 33]. The proposed model includes a dynamical driver triggering non-systematically dry conditions, namely the *ENSO dynamics*, that in turn interacts with and influences TCWV dynamics and precipitation patterns in Southeast Asia. While many models of *ENSO dynamics* exist, the Jin-Timmermann model [22, 23] is widely used in climate science as a first approximation of the chaotic dynamics of ENSO. The model considers the interactions between the ocean and the atmosphere, and includes various feedback mechanisms that influence the evolution of ENSO. It reads:

$$\begin{aligned}
\dot{x} &= \rho\delta(x^2 - ax) + x(x + y + c - c\tanh(x + z)) + \sigma_x\eta_t, \\
\dot{y} &= -\rho\delta(ay + x^2) \\
\dot{z} &= \delta(k - z - \frac{x}{2}),
\end{aligned} \tag{1}$$

where $\eta_t \sim N(0, 1)$, $\delta = 0.225423$, $\rho = 0.3224$, $c = 2.3952$, $k = 0.4032$, $a = 7.3939$, $\sigma_x = 0.01$, $\kappa = 0.85$. The variables x, $y < 0$ and z are rendered dimensionless equivalent of the Western to Eastern pacific temperature difference, i.e. a proxy for ENSO strength (x), the Western pacific temperature (y) and the oceanic circulation strength (z). As clear from above, the model is stochastic in nature, which means that it incorporates random processes to simulate the inherent variability of ENSO given by the oceanic eddies. In the phase-space of this reduced order model strong El Niño events can be identified by $x > -1$ as suggested in [23]. Given the model for ENSO we need to reduce the dynamics of TCWV in Southeast Asia. In order to do so, we exploit the simplest model featuring a gradient dynamics in a double well potential for the variable u. In our study, the two states of u in the potential represent the precipitation anomalies over Southeast Asia, with one state (u positive) corresponding to typical precipitation patterns associated with convection and another state (u negative) representing drier conditions than average. The potential depends on y that mimics the temperature anomaly over the Western Pacific: when y, that is negatively defined, approaches zero, we get suppression of convection, when y is negative convection can be triggered. This feature captures the bimodal distribution of precipitation patterns over Southeast Asia and allows us to simulate the

transitions between the two states in response to ENSO variability. We describe a perturbed double-well potential dynamics for the model of the dry-wet state switching as

$$\dot{u} = -\frac{\partial V_y(u)}{\partial u} + \sigma_u \xi_t, \qquad \text{with} \tag{2a}$$

$$V_y(u) = -\frac{1}{2}u^2 + \frac{1}{4}u^4 - \epsilon(y+\kappa)u, \tag{2b}$$

and where $\xi_t \sim N(0,1)$, and y is the temperature of the Western Pacific governed by the Jin-Timmermann model described above. We have ϵ (strength of effects from ENSO dynamics), and σ_u (strength of external noise) as control parameters. It is important to underline that the presence of a linear term in the potential function determines an asymmetry of the two states and the sign of the corresponding coefficient is usually inspected as a potential source of a tipping point (leading to a saddle-node bifurcation). In our model, the sign and the value is related to the dynamic variable y, thus directly pointing out the role of the Western pacific temperature in leading El Niño events. By performing linear stability analysis to our 4-dimensional model in absence of noise ($\sigma_x = \sigma_u = 0$) three different fixed points can be depicted, only dependent on the forcing ϵ and the parameter κ.

This approach is similar to the standard stochastic resonance model [36], but with a linear term added to account for transitions between asymmetric states with varying probabilities and residence times. However, its core mechanism is fundamentally different. The key innovation lies in the fact that drought occurrence is now governed by stochastic-chaotic interactions rather than stochastic-periodic ones.

IV. RESULTS

The attractor generated by the model in (1), with parameters detailed in the methods section, is shown in Fig. 2b. The model captures convection dynamics, showing that wet states recur more frequently due to spontaneous convection in tropical systems. Strong El Niño events ($x > -1$; see [23]) may trigger prolonged dry periods, occasionally lasting longer than the El Niño event itself. The fraction of very dry states(u< -0.5) over total number of states in the model is 0.02, comparable with that of the real data.

This behavior corresponds to a model limit cycle, a periodic orbit in the state space to which nearby trajectories converge to, either leading into an El Niño phase or allowing exit from it. In the first scenario, the stochastic potential well remains unaffected, and the system continues oscillating between wet and dry states. In the second, the dry state persists continuously, precluding a return to wet conditions. This explains the model's ability to capture prolonged dry spells.

For a quantitative comparison, we apply persistence and dimensional analyses to the model outputs (Fig. 2b). The behavior of the model in d-θ space resembles that of observed data, where low dimensionality and high persistence correspond to strong El Niño events. The more distinct separation of blue and red points in Fig. 2c,d compared to Fig. 1b reflects the model's overall reduced complexity, indicated by a lower average and maximum instantaneous dimension. Nonetheless, the key features of the d-θ space—specifically, the shape of the point cloud in the diagram and the association of low-dimensional, highly persistent states with positive ENSO index values that exhibit greater persistence at similar d levels—are accurately captured by the model.

To better understand how the proposed stochastic model behaves, we perform a number of runs for different model parameters, focusing in particular on σ_x, ϵ, and σ_u. The parameter σ_x controls the noise of the ENSO dynamics in the Jin-Timmerman model, while ϵ and σ_u represent the modulation strength of ENSO and external noise on the dry-wet state dynamics described by the double-well potential ((2)), respectively.

Fig. 3 shows two runs of our stochastic model for $\sigma_x = 0$ (no noise in the ENSO dynamics) in red, and for $\sigma_x = 0.1$ (noise in the ENSO dynamics) in blue. The other two parameters related to the dry-wet state dynamics are instead fixed: $\epsilon = 2$ and $\sigma_u = 0.3$. Fig. 3a shows the ENSO part of the model with a projection of the phase portrait on

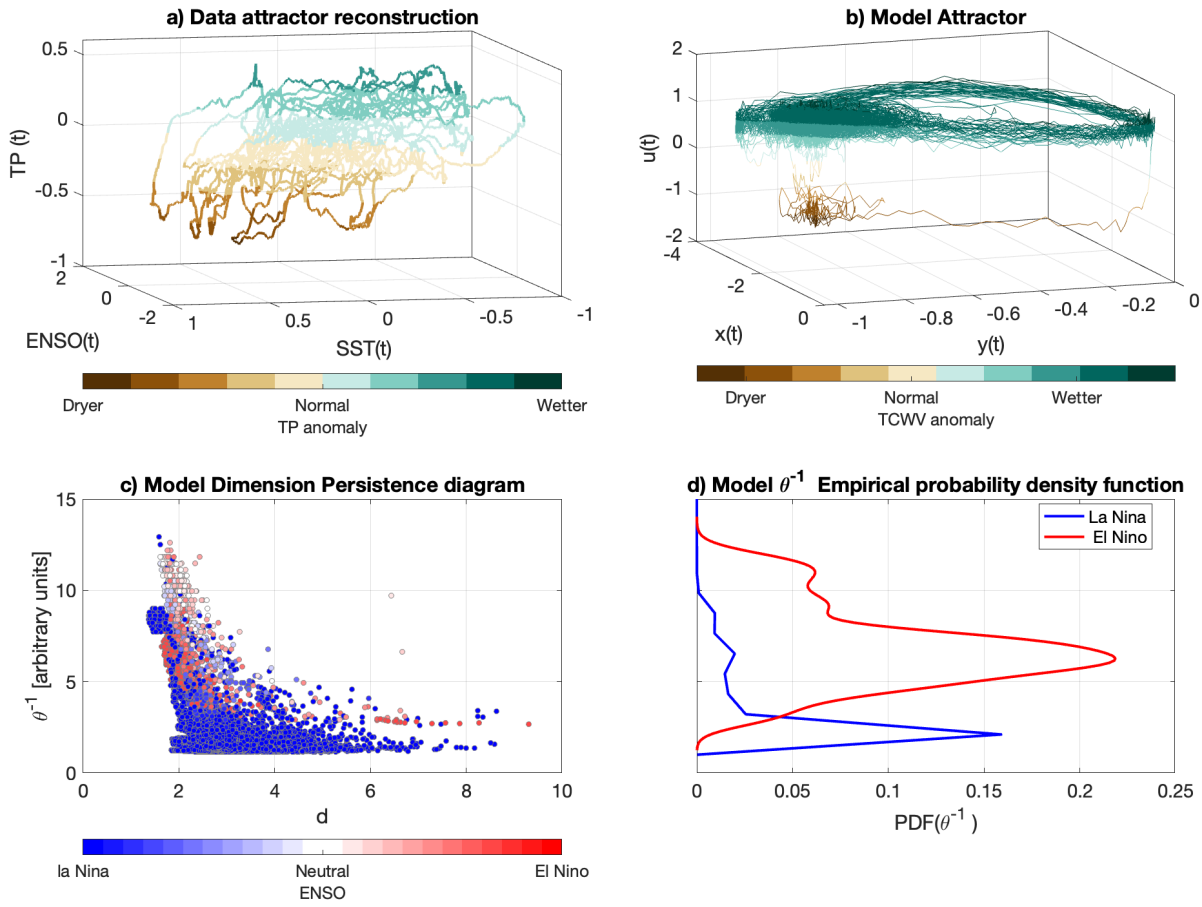

FIG. 2. **Comparison of reanalysis data and model outputs embedded in a three-dimensional space.** (a) Attractor derived from embedding observed $TCWV(t)$, Niño3.4 index $ENSO(t)$, and Western Equatorial Pacific $SST(t)$. (b) Attractor generated by the model using Eq. 1 and parameters specified in the Materials and Methods. (c) Dimension-persistence diagram for the model run, with each state colored by their corresponding $ENSO(t)$ value. (d) Empirical probability density function of persistence for El Niño ($ENSO(t) > 0$) and La Niña ($ENSO(t) < 0$) phases.

x, y, z, while Fig. 3b shows the dynamics of precipitation anomalies u vs time t. The cyan-colored dots represent states with precipitation anomalies $u < -1$ – i.e., dry conditions.

In order to better understand the proposed stochastic model, we explore its parametric space by performing 100 realizations of the model, each consisting of 10^6 iterations with $dt = 10^{-4}$. The fraction of time spent in wet states (Figs. 4a,b) increases with increasing σ_u and/or ϵ, and saturates at around a 60–70% occurrence of the wet state. Instead, the average number of transitions (Fig. 4c) and the standard deviation of the number of transitions (Fig. 4d) depend solely on σ_u. Finally, the average residence time (or time cluster size) in the wet or dry states decrease when increasing $\sigma_u > 0.5$ (Fig. 4e,f), i.e. for large values of σ_u the dynamics is driven by noise and jump rapidly from wet to dry states and viceversa.

DISCUSSION

The residence time in each state of our model decreases with increasing σ_u. These results allow drawing some parallels with the results expected with climate change where we would expect that the large availability of moisture and heat will increase the convective potential (here mimicked by increase of σ_u) and this will cause a larger variability

of precipitation in the region, coherently with what reported in IPCC AR6 [37]. The role of El Niño is less trivial: If climate change increases the coupling between atmospheric and oceanic variables (indicated by a higher ϵ), this would introduce a dynamic competition between two opposing effects: on the one hand, the increased coupling could amplify feedback mechanisms within the coupled system, intensifying both dry and wet extremes depending on the phase of phenomena such as ENSO (El Niño-Southern Oscillation); on the other hand, the warming atmosphere, capable of holding more moisture, would generally drive the climate toward a wetter state with more frequent and intense precipitation events. This competition implies that while an overall wetter climate may be expected, regions may still experience heightened variability, with the possibility of both intensified droughts and rainfall extremes arising from the enhanced coupling. This is also coherent with the results reported for the region in the IPCC AR6 report [37], and it is captured by our model thanks to the role of the asymmetric double-well potential in modifying the nature of the fixed points of the Jin-Timmermann model. Indeed, (1) in absence of noise ($\sigma_u = 0$) admits an unstable saddle point ($u^\star$) depending on the Western Pacific temperature (y), which in turn depends on El Niño phase (x). By looking at the mathematical solutions of the model, we find that the dry state ($u < -1$) is not approached, unless the noise term in the ENSO dynamics (σ_x) is turned on. In that case, the deterministic dynamics, comprising the limit cycle dynamics characterizing an El Niño event and an unstable saddle point ($x = 0$), is stochastically driven by the precipitation to induce bifurcations between wet and dry states, favoring the wet ones. This means that if there are no fluctuations on a smaller scale than ENSO, which we model here with noise, the dynamics of El Niño phase (x) alone, which influences that of the Western Pacific temperature (y), cannot generate wet-dry transitions. Furthermore, with external noise on the dry-wet state (σ_u) different from noise on ENSO (σ_x), the dynamics dynamics of u is more stable if σ_u is small. Therefore, ENSO phase changes (x) alone cannot induce the switch between the wet and dry states. The interaction between strong El Niño events and prolonged dry conditions over Southeast Asia is a complex phenomenon resulting from a combination of atmospheric and oceanic processes. Our study demonstrates that this link can be effectively modeled using a low-dimensional system of equations featuring a rare basin of attraction, mimicking prolonged dry conditions over Southeast Asia. This basin is statistically more likely to be reached during the strongest El Niño events,

The stochasticity of the prolonged dry events also presents challenges for predicting their occurrence and intensity, making it difficult to develop effective adaptation strategies. Moreover, our model suggests that changing control climatic parameters can lead to a switch to dry conditions becoming more frequent than wet ones. Although we do not investigate here whether this results in a hysteresis loop or irreversible changes, the behaviour is nonetheless reminiscent of a climate tipping (see, Ref. [38] for an example of a tipping point related to ENSO). The information derived from our model suggests that early-warning systems should place particular focus on skill in predicting the possibility of prolonged dry states. In summary, our study provides insights into the link between strong El Niño events and prolonged dry conditions over Southeast Asia, highlighting the complex yet statistically predictable nature of these events. The latter is dictated by the effect of perturbations of both stochastic and deterministic, albeit chaotic, origin to the dynamics that determines the wet or dry state of the region under study. By continuing to investigate the underlying processes and developing accurate probabilistic prediction models, we can better prepare for and mitigate the impacts of future El Niño events on the region.

CONCLUSIONS

Our study reveals a complex and stochastic relationship between strong El Niño events and prolonged dry conditions in Southeast Asia. Through a novel mathematical model that couples ENSO dynamics with a bi-stable stochastic system, we show how strong El Niño phases can lead to extended periods of dryness. The model's ability to replicate the observed persistence of these conditions highlights the importance of stochastic interactions in climate dynamics and reinforces the challenge of predicting individual dry events. Importantly, this work suggests that climate change may intensify these stochastic dry events, underscoring the need for robust early-warning systems tailored to anticipate

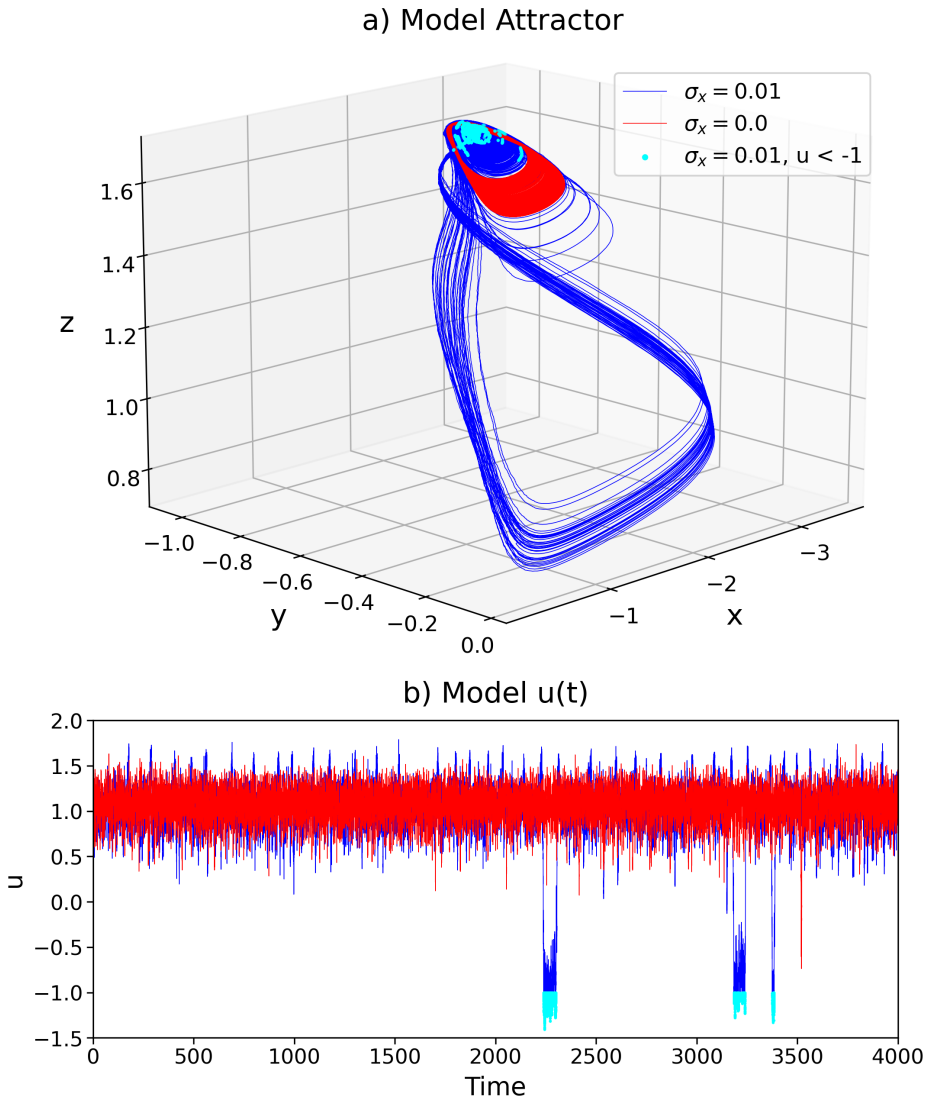

FIG. 3. **Two runs of the stochastic model illustrating the impact of noise in ENSO dynamics.** The red curve represents the model run with $\sigma_x = 0$ (no noise in ENSO dynamics), while the blue curve corresponds to $\sigma_x = 0.1$ (with noise in ENSO dynamics). For both runs, the parameters related to the dry-wet state dynamics are fixed at $\epsilon = 2$ and $\sigma_u = 0.3$. Panel (a) displays the ENSO component of the model with a projection of the phase portrait on x, y, z coordinates. Panel (b) shows the evolution of precipitation anomalies u over time t, with cyan-colored dots indicating states where precipitation anomalies $u < -1$, corresponding to dry conditions.

prolonged dry spells. Future studies could build on these findings to further explore potential climate tipping points, improving predictive accuracy and resilience planning for regions facing similar climatic hazards. In this study, we propose a minimal model that provides a novel perspective on the relationship between prolonged dry spells and El Niño events. While multiple models could potentially capture this link, our model has the distinct advantage of minimalism, capitalizing on the inherent chaotic dynamics of El Niño. This approach shifts the paradigm from traditional models—often probabilistic or driven by stochastic resonance—toward a new class where transitions are governed by chaos. By embracing this chaotic framework, we offer an alternative, more mechanistic explanation for the co-occurrence of strong ENSO events and prolonged dry conditions, rooted in the intrinsic dynamics of the climate system rather than random chance.

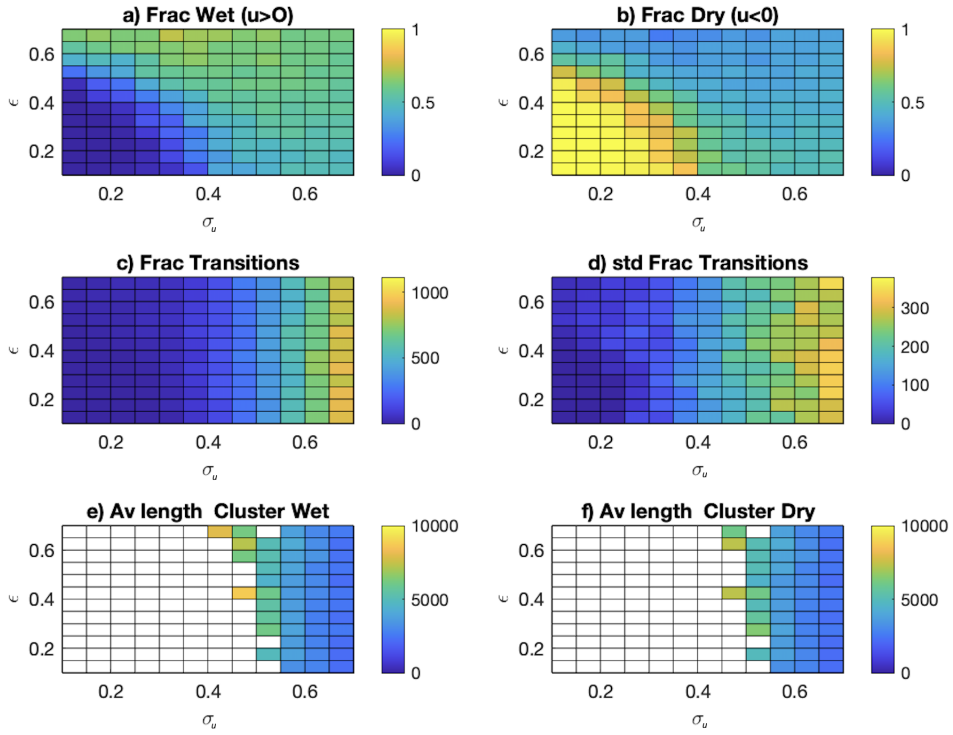

FIG. 4. **Phase diagram of the model for $\sigma_u \in (0, 0.8)$, $\epsilon \in (0.1, 0.9)$.** Fraction of time spent in the wet a) or dry b) states. Average c) and Standard deviation d) of the number of transitions. Average cluster length (in days) in the wet e) and dry f) states.

Appendix A: Understanding Dimension and Persistence in Geophysical Systems

In this section of the supplementary material, we expand on the concepts of dimension and persistence used in the main text to characterize the behavior of complex, high-dimensional systems such as climate phenomena influenced by El Niño events. These concepts come from dynamical systems theory and extreme value theory (EVT) and are tools for analyzing geophysical data, even when the available data series are short or incomplete. When studying a system with a complex attractor, as often encountered in climate science, it is useful to characterize the attractor's geometry using state-dependent indicators that can be easily computed from finite-size observations. In this supplementary material, we provide additional information on the local dimensions d and the local persistence θ used in the article. A full description of these metrics can be found in [31].

1. Dimension and Persistence in Complex Systems

The local dimension, denoted by $d_\mu(x)$, measures how densely populated the phase space is near a given state x. In simpler terms, it reflects the variety of possible configurations that the system can occupy around a specific point. Formally, it's defined as:

$$d_\mu(x) = \lim_{r \to 0} \frac{\log \mu(B(x, r))}{\log r}, \tag{A1}$$

where $B(x, r)$ represents a ball of radius r centered at x, and $\mu(B(x, r))$ is the measure (or "density") of states within this ball.

However, in practical applications, we can only approximate this measure due to the finite length of real-world

data. Therefore, we use an "effective" or pre-asymptotic version, defined as:

$$d_{\mu,r}(x) = \frac{\log \mu(B(x,r))}{\log r}, \tag{A2}$$

which converges to the system's information dimension D_1 as r approaches zero. For most geophysical systems, which have multifractal structures, the local dimension varies across different regions of the attractor, providing a spectrum of dimensions rather than a single value. The local dimension $d_{\mu,r}(x)$ tells us about the recurrence properties of the system, or how frequently the system revisits states near x. Lower values of $d_{\mu,r}$ suggest that the system tends to return more often to regions around x, indicating a dense region of the attractor. Conversely, higher values indicate sparser regions, which are less frequently revisited.

This property is particularly helpful in climate research, where scientists are often interested in the recurrence of specific patterns, such as the development of dry conditions in response to El Niño events. By calculating the local dimension, researchers can identify which atmospheric configurations are more persistent and which are rare, helping to predict the likelihood of extreme conditions.

While local dimension inform on the density of states near a given point, persistence is a measure of how long the system remains in a particular state before transitioning to another. In our study, persistence is particularly relevant for understanding prolonged dry conditions, as it quantifies the duration of these states.

Persistence is estimated through a quantity known as the extremal index θ indicates how clustered extreme events are. If θ is low, extreme events like dry periods are likely to cluster together, resulting in longer durations for these conditions. Persistence is therefore complementary to local dimension: while local dimension captures the recurrence and density, persistence captures the timescales associated with these states.

In combination, dimension and persistence offer a powerful framework for studying climate dynamics, especially when faced with partial or finite data. The two measures are connected through large deviations theory, which describes how much the observed values of $d_{\mu,r}(x)$ deviate from the typical information dimension D_1. These deviations provide additional information into the variability and stability of the system.

For example, in the context of El Niño, regions of the phase space with low $d_{\mu,r}(x)$ and high persistence may correspond to stable dry conditions. The variability observed around these regions is described by a large deviations principle, which quantifies the probability of seeing atypical behaviors (e.g., unusually long dry periods) in these otherwise stable states.

In real-world applications, observations from geophysical systems are often partial. For instance, when measuring atmospheric conditions, only a subset of variables or locations can be recorded. This partial observation can be represented by an observable function $f : M \to R^k$, where M is the phase space, and R^k is the space of observed variables.

The observable f essentially projects the full dynamics onto a reduced space, capturing a subset of the system's behavior. For such projections, the local dimension $d_{\mu_f}(f(x))$ is given by:

$$d_{\mu_f}(f(x)) = \min(k, d_\mu(x)), \tag{A3}$$

where k is the dimension of the observed space. This result implies that if the observed dimension k is smaller than the local dimension $d_\mu(x)$, some structural information about the attractor is lost. Conversely, if k is large enough, the local dimension of the attractor is preserved in the projection.

This approach allows scientists to study complex systems using simplified representations, while retaining important characteristics of the full system's behavior.

Appendix B: Justification of observable selection

In our study, we aim to use one variable to describe the wet/dry state of Southeast Asia that has a significant modulation on regional prolonged dry conditions. The most straightforward variable to consider is total precipitation; however, it has a very sparse field with high gradients. These characteristics make it unsuitable for methods based on analogues (i.e., maps that have similar configuration), as it is difficult to find true analogues in such sparse fields. To this end, we selected total column water vapor (TCWV) as the observable for analysis in the main text. TCWV is a crucial variable that characterizes atmospheric moisture content and is closely related to precipitation, as accumulated water vapor increases the potential for precipitation, particularly in tropical regions [39]. To further demonstrate the correlation between TCWV and TP and validate the choice of using TCWV as the observable, we plotted the time series of the average TCWV and TP over Southeast Asia [90°E–140°E, 10°S–20°N] (Fig. 5). As expected, they exhibited a high Pearson correlation (0.76 for both the 30-day moving average and the 365-day moving average).

In Figure 8, we present the results obtained from the same analysis as in Figure 1, but using TP as the observable instead of TCWV. TP exhibit much higher local dimension d and lower persistence θ^{-1} than TCWV, suggesting more complicated and less predictable dynamics. Interestingly, despite TP being considered unsuitable for computing dynamical indices, we can still observe an increase in persistence during the strongest El Niño events. The composite anomaly maps of the most persistent fields also show drier conditions over Southeast Asia compared to the least persistent states.

Appendix C: Appendix Figures

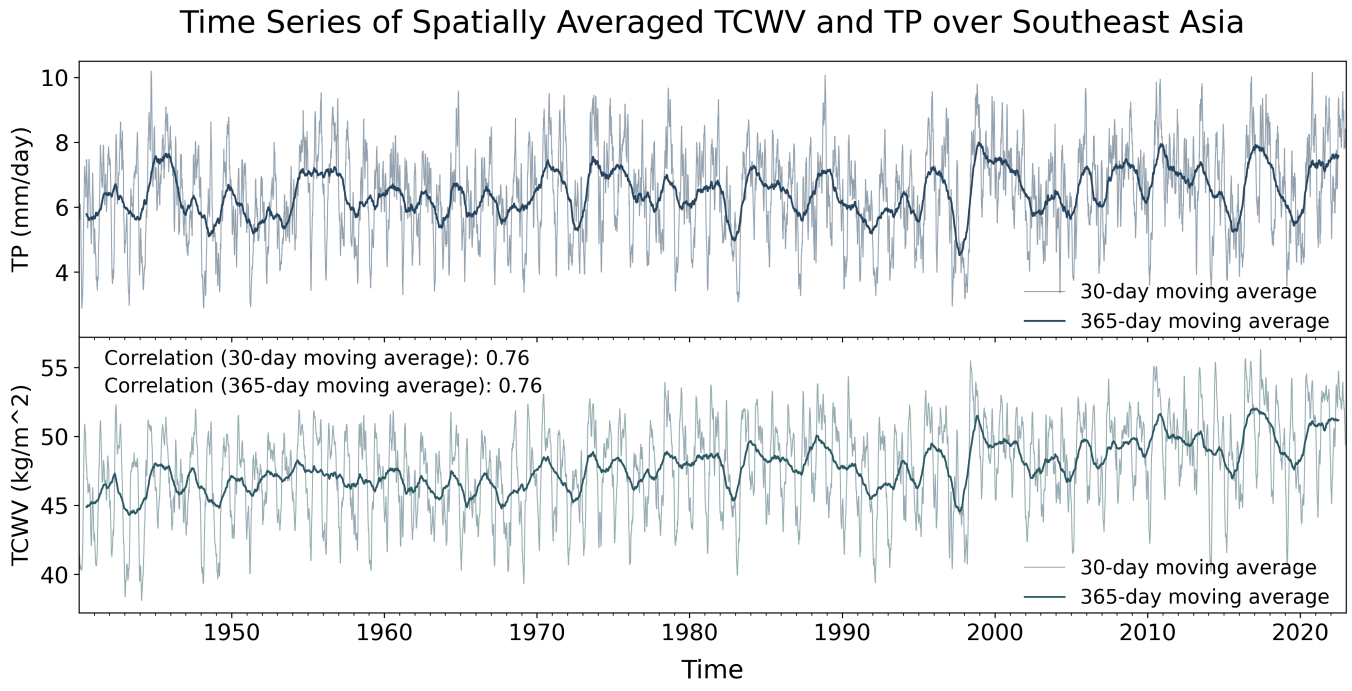

FIG. 5. **Time series of spatially averaged TCWV and TP over Southeast Asia.** The thin line represents the 30-day moving average, while the thick line shows the 365-day moving average.

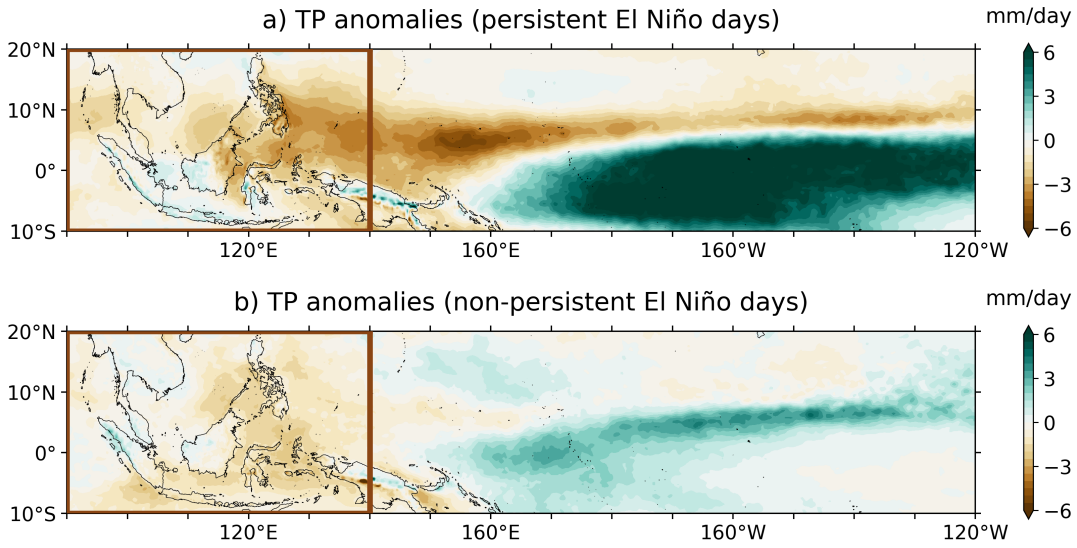

FIG. 6. **Dynamical analysis for the total column water vapour (TCWV) field from ERA5 data.** (a) and (b) correspond to (c) and (d) in Figure 1, but present the composite anomaly of TP instead of TCWV.

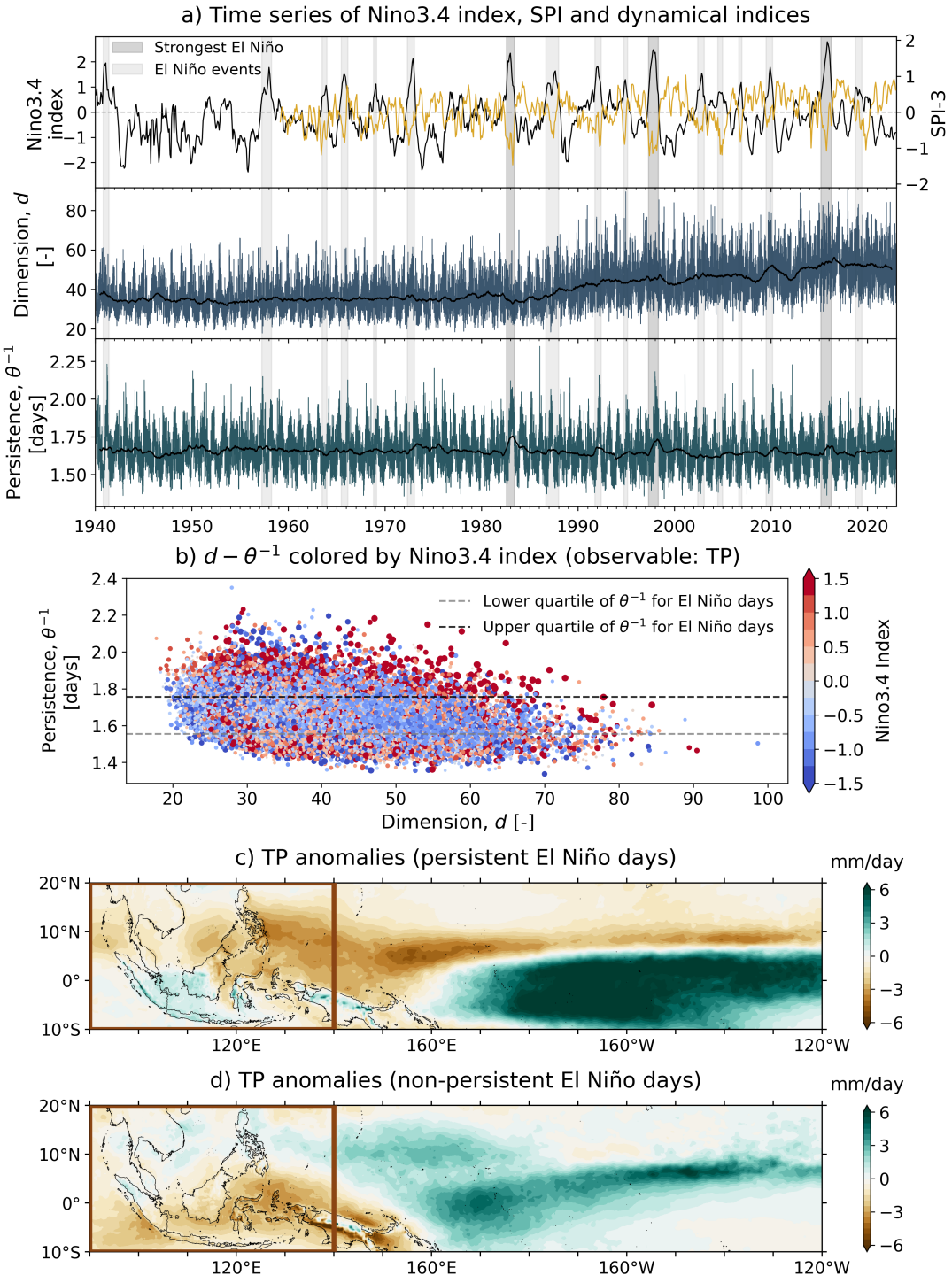

FIG. 7. **Dynamical analysis for the total precipitation (TP) field from ERA5 data.** As in Figure 1, but using TP as observable.

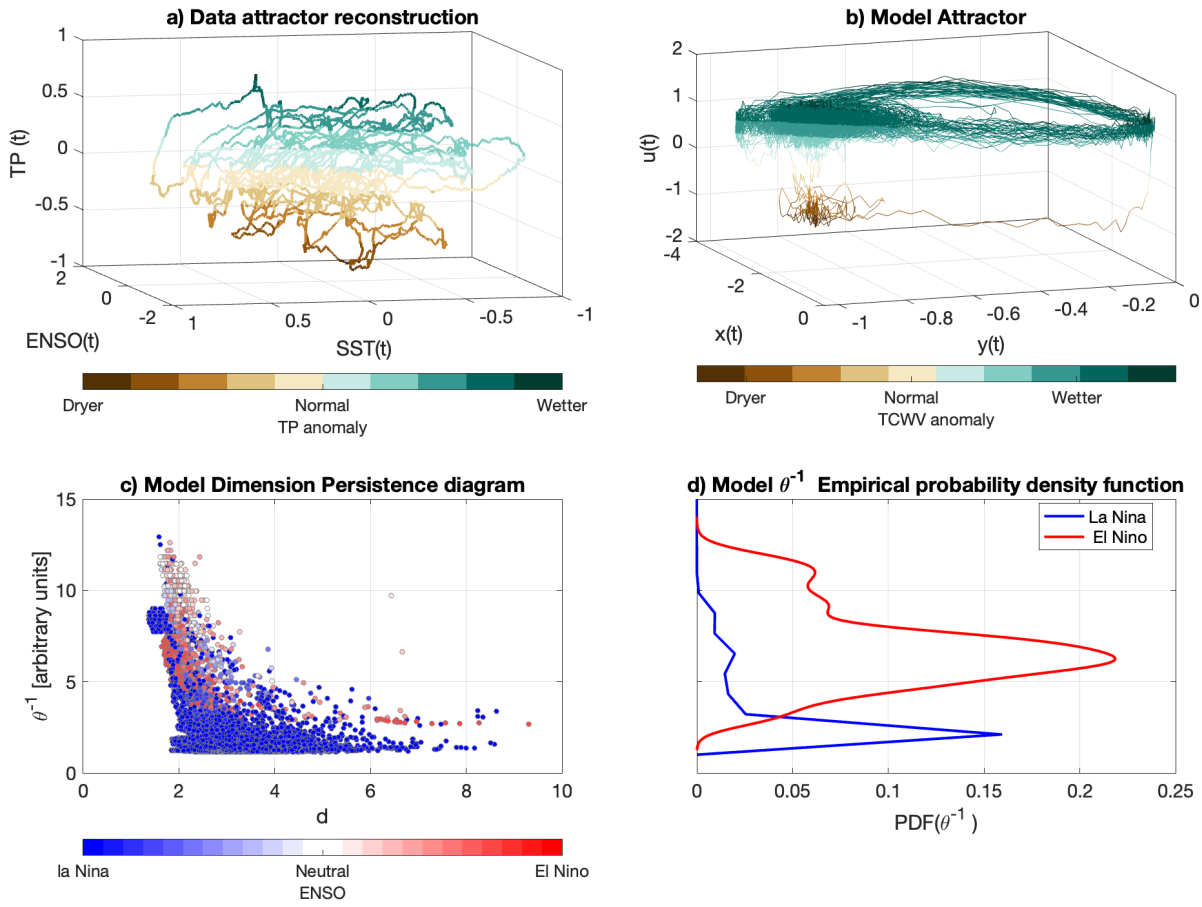

FIG. 8. **Attractor obtained embedding real data in a three dimensional space.** As in Figure 2, but using the time series of TP instead of TCWV to reconstruct the attractor.

ACKNOWLEDGMENTS

This study received support from the European Union's Horizon 2020 research and innovation programme under grant agreement No. 101003469 (XAIDA) and from the European Union's Horizon 2020 Marie Sklodowska-Curie grant agreement No. 956396 (EDIPI) and the LEFE-MANU-INSU-CNRS grant "CROIRE". The authors benefited from state aid managed by the National Research Agency under France 2030 bearing the references ANR-22-EXTR-0005 (TRACCS-PC4-EXTENDING project), and acknowledge support from the "COESION" project funded by the French National program LEFE (Les Enveloppes Fluides et l'Environnement) and project nr. 2022-06599 funded by the Swedish Research Council Vetenskapsrådet.

[1] S. G. H. Philander, El Niño southern oscillation phenomena, Nature **302**, 295 (1983).

[2] C. Wang, Three-ocean interactions and climate variability: a review and perspective, Climate Dynamics **53**, 5119 (2019).

[3] R. Kane, El Niño timings and rainfall extremes in India, southeast Asia and China, International Journal of Climatology: A Journal of the Royal Meteorological Society **19**, 653 (1999).

[4] S. Yoshida, T. Morimoto, T. Ushio, and Z. Kawasaki, ENSO and convective activities in Southeast Asia and western Pacific, Geophysical Research Letters **34** (2007).

[5] Y. Fan, K. Fan, X. Zhu, and K. Fraedrich, El Niño–related summer precipitation anomalies in Southeast Asia modulated by the Atlantic multidecadal oscillation, Journal of Climate **32**, 7971 (2019).

[6] C. Dong, R. Noyelle, G. Messori, A. Gualandi, L. Fery, P. Yiou, M. Vrac, F. D'Andrea, S. J. Camargo, E. Coppola, G. Balsamo, C. Chen, D. Faranda, and G. Mengaldo, Indo-pacific regional extremes aggravated by changes in tropical weather patterns, Nature Geoscience (2024).

[7] L. Juneng and F. T. Tangang, Evolution of ENSO-related rainfall anomalies in Southeast Asia region and its relationship with atmosphere–ocean variations in Indo-Pacific sector, Climate Dynamics **25**, 337 (2005).

[8] M. E. Marlier, R. S. DeFries, A. Voulgarakis, P. L. Kinney, J. T. Randerson, D. T. Shindell, Y. Chen, and G. Faluvegi, El Niño and health risks from landscape fire emissions in southeast Asia, Nature climate change **3**, 131 (2013).

[9] R. Gan, Q. Liu, G. Huang, K. Hu, and X. Li, Greenhouse warming and internal variability increase extreme and central Pacific El Niño frequency since 1980, Nature Communications **14**, 394 (2023).

[10] O. Alizadeh, M. Qadimi, M. Zolghadrshojaee, and P. Irannejad, Frequency of different types of El Niño events under global warming, International Journal of Climatology **42**, 9697 (2022).

[11] K. Thirumalai, P. N. DiNezio, Y. Okumura, and C. Deser, Extreme temperatures in Southeast Asia caused by El Niño and worsened by global warming, Nature communications **8**, 15531 (2017).

[12] I. P. on Climate Change, *Climate Change 2021: The Physical Science Basis. Contribution of Working Group I to the Sixth Assessment Report of the Intergovernmental Panel on Climate Change*, edited by V. Masson-Delmotte, P. Zhai, A. Pirani, S. L. Connors, C. Péan, S. Berger, N. Caud, Y. Chen, L. Goldfarb, M. I. Gomis, M. Huang, K. Leitzell, E. Lonnoy, J. B. R. Matthews, T. K. Maycock, T. Waterfield, O. Yelekçi, R. Yu, and B. Zhou (Cambridge University Press, Cambridge, United Kingdom and New York, NY, USA, 2021) in press.

[13] C. J. Muller, L. E. Back, P. A. O'Gorman, and K. A. Emanuel, A model for the relationship between tropical precipitation and column water vapor, Geophysical Research Letters **36** (2009).

[14] D. Faranda, G. Messori, and S. Vannitsem, Attractor dimension of time-averaged climate observables: insights from a low-order ocean-atmosphere model, Tellus A: Dynamic Meteorology and Oceanography **71**, 1 (2019).

[15] T. Alberti, F. Daviaud, R. V. Donner, B. Dubrulle, D. Faranda, and V. Lucarini, Chameleon attractors in turbulent flows, Chaos, Solitons & Fractals **168**, 113195 (2023).

[16] A. Gualandi, J.-P. Avouac, S. Michel, and D. Faranda, The predictable chaos of slow earthquakes, Science advances **6**, eaaz5548 (2020).

[17] A. Gualandi, D. Faranda, C. Marone, M. Cocco, and G. Mengaldo, Deterministic and stochastic chaos characterize laboratory earthquakes, Earth and Planetary Science Letters **604**, 117995 (2023).

[18] D. Faranda, Y. Sato, G. Messori, N. R. Moloney, and P. Yiou, Minimal dynamical systems model of the northern hemisphere jet stream via embedding of climate data, Earth System Dynamics **10**, 555 (2019).

[19] G. Messori, N. Harnik, E. Madonna, O. Lachmy, and D. Faranda, A dynamical systems characterisation of atmospheric jet regimes, Earth System Dynamics Discussions **2020**, 1 (2020).

[20] C. Dong, G. Messori, D. Faranda, A. Gualandi, V. Lucarini, and G. Mengaldo, Spatial indices reveal scale-dependent atmospheric dynamics, arXiv preprint arXiv:2412.10069 (2024).

[21] C. Dong, D. Faranda, A. Gualandi, V. Lucarini, and G. Mengaldo, Revisiting the predictability of dynamical systems: a new local data-driven approach, arXiv preprint arXiv:2409.14865 (2024).

[22] J. Guckenheimer, A. Timmermann, H. Dijkstra, and A. Roberts, (Un)predictability of strong El Niño events, Dynamics and Statistics of the Climate System **2**, dzx004 (2017).

[23] D. Lucente, C. Herbert, and F. Bouchet, Committor Functions for Climate Phenomena at the Predictability Margin: The Example of El Niño–Southern Oscillation in the Jin and Timmermann Model, Journal of the Atmospheric Sciences **79**, 2387 (2022).

[24] H. Hersbach, B. Bell, P. Berrisford, S. Hirahara, A. Horányi, J. Muñoz-Sabater, J. Nicolas, C. Peubey, R. Radu, D. Schepers, *et al.*, The ERA5 global reanalysis, Quarterly Journal of the Royal Meteorological Society **146**, 1999 (2020).

[25] I. M. Held and B. J. Soden, Robust responses of the hydrological cycle to global warming, Journal of climate **19**, 5686 (2006).

[26] Q. Jiang, W. Li, Z. Fan, X. He, W. Sun, S. Chen, J. Wen, J. Gao, and J. Wang, Evaluation of the era5 reanalysis precipitation dataset over chinese mainland, Journal of hydrology **595**, 125660 (2021).

[27] B. Huang, P. W. Thorne, V. F. Banzon, T. Boyer, G. Chepurin, J. H. Lawrimore, M. J. Menne, T. M. Smith, R. S. Vose, and H.-M. Zhang, Extended reconstructed sea surface temperature, version 5 (ERSSTv5): upgrades, validations, and intercomparisons, Journal of Climate **30**, 8179 (2017).

[28] X. Zhang, A dataset of monthly SPI and SPEI derived from ERA5 over 1959-2022 10.6084/m9.figshare.24485389.v1 (2023).

[29] T. Phan-Van, P. Nguyen-Ngoc-Bich, T. Ngo-Duc, T. Vu-Minh, P. V. Le, L. Trinh-Tuan, T. Nguyen-Thi, H. Pham-Thanh, and D. Tran-Quang, Drought over southeast asia and its association with large-scale drivers, Journal of Climate **35**, 4959 (2022).

[30] D. Faranda, G. Messori, and P. Yiou, Dynamical proxies of north atlantic predictability and extremes, Scientific reports **7**, 41278 (2017).

[31] D. Faranda, G. Messori, T. Alberti, C. Alvarez-Castro, T. Caby, L. Cavicchia, E. Coppola, R. V. Donner, B. Dubrulle, V. M. Galfi, E. Holmberg, V. Lembo, R. Noyelle, P. Yiou, B. Spagnolo, D. Valenti, S. Vaienti, and C. Wormell, Statistical physics and dynamical systems perspectives on geophysical extreme events, Phys. Rev. E **110**, 041001 (2024).

[32] D. Faranda, Y. Sato, B. Saint-Michel, C. Wiertel, V. Padilla, B. Dubrulle, and F. Daviaud, Stochastic chaos in a turbulent swirling flow, Physical review letters **119**, 014502 (2017).

[33] A. Timmermann, F.-F. Jin, and J. Abshagen, A nonlinear theory for el niño bursting, Journal of the atmospheric sciences **60**, 152 (2003).

[34] C. Penland and L. Matrosova, Studies of el niño and interdecadal variability in tropical sea surface temperatures using a nonnormal filter, Journal of climate **19**, 5796 (2006).

[35] Y. Wang, B. Wang, and J.-H. Oh, Impact of the preceding el niño on the east asian summer atmosphere circulation, Journal of the Meteorological Society of Japan. Ser. II **79**, 575 (2001).

[36] R. Benzi, G. Parisi, A. Sutera, and A. Vulpiani, Stochastic resonance in climatic change, Tellus **34**, 10 (1982).

[37] R. P. Allan, E. Hawkins, N. Bellouin, and B. Collins, IPCC, 2021: summary for Policymakers, Cambridge University Press (2021).

[38] M. Duque-Villegas, J. F. Salazar, and A. M. Rendón, Tipping the enso into a permanent el niño can trigger state transitions in global terrestrial ecosystems, Earth System Dynamics **10**, 631 (2019).

[39] C. S. Bretherton, M. E. Peters, and L. E. Back, Relationships between water vapor path and precipitation over the tropical oceans, Journal of climate **17**, 1517 (2004).